Inorg. Chem. **2006**, *45*, 3557−3568

Synthesis, Molecular and Electronic Structure, and TDDFT and TDDFT-PCM Study of the Solvatochromic Properties of $(Me_2Pipdt)Mo(CO)_4$ Complex (Me_2Pipdt = *N,N′*-Dimethylpiperazine-2,3-dithione)

Victor N. Nemykin,*[†,‡] Joseph G. Olsen,[†] Eranda Perera,[‡] and Partha Basu*[‡]

Department of Chemistry and Biochemistry, University of Minnesota at Duluth, Duluth, Minnesota 55812, and Department of Chemistry and Biochemistry, Duquesne University, Pittsburgh, Pennsylvania 15282

Received September 26, 2005

The synthesis, spectroscopic, and structural characterization of the $(Me_2Pipdt)Mo(CO)_4$ complex (Me_2Pipdt = *N,N′*-piperazine-2,3-dithione) are presented in this paper. The title complex crystallizes in the $P2_1/n$ space group with a = 25.541(3) Å, b = 10.3936(14) Å, c = 10.9012(12) Å, β = 92.261(9)°, V = 2891.6(6) Å^3, and Z = 8. Gas- and solution-phase structural and electronic features of $(Me_2Pipdt)Mo(CO)_4$ and Me_2Pipdt have been investigated using density functional theory. The molecular structure underscores the flexibility of the NC(S)C(S)N fragment in both the free ligand and the metal complex. On the basis of structural, spectroscopic, and theoretical results, the bidentate ligand in $(Me_2Pipdt)Mo(CO)_4$ is considered to be in the dithione, not dithiolate, form. Time-dependent density functional theory has been used for the investigation of the excited states and solvatochromic properties of $(Me_2Pipdt)Mo(CO)_4$. The calculated vertical excitation energies in solution are consistent with the experimental data, showing that the metal-to-ligand charge-transfer transitions, in both the visible and UV regions, dominate over the ligand-based π–π^* transitions.

Introduction

Since their initial discovery, metallodithiolenes have been intensively investigated, in part because of their potential applications in many areas such as nonlinear optics, light-driven information devices, laser dyes, and sensors.[1−5] In contrast, the finding of dithiolenes in biological systems is a relatively recent event.[6] The first chemical evidence of the presence of metallodithiolenes in enzymes was reported in the mid-1980s, followed by the crystallographical characterization of a tungsten enzyme about 10 years ago, and then several structural reports on molybdenum enzymes followed.[6−9] To date, more than 50 molybdenum enzymes have been reported to contain a metallodithiolene unit as their active site. The bidentate dithiolene ligand can coordinate to molybdenum, forming mono-, bis-, or triscomplexes. Among these, the presence of both mono- and bis(metallodithiolene) complexes has been confirmed in biological systems,[6−8,10] while a trischelated molybdenum center in biological systems has not yet been reported. The dithiolene unit in these enzymes constitutes a part of the cofactor that also has a reduced heterocycle ring, which provides a conformational flexibility of the pyranopterin ligand.[7]

Molybdenum dithiolene moieties can display various redox levels because both the metal and ligand are potentially redox-active (Figure 1). The ability to display variable redox states undoubtedly influences the overall function of the molybdenum dithiolene enzymes. Many researchers have contributed to the development of a molecular-level description of these essential enzymes by synthesizing new mol-

* To whom correspondence should be addressed. E-mail: vnemykin@d.umn.edu (V.N.N.), basu@duq.edu (P.B.).
[†] University of Minnesota at Duluth.
[‡] Duquesne University.

(1) Faulmann, C.; Cassoux, P. *Prog. Inorg. Chem.* **2003**, *52*, 399−489.
(2) Pilato, R. S.; Van Houten, K. A. *Prog. Inorg. Chem.* **2003**, *52*, 369−397.
(3) Cummings, S. D.; Eisenberg, R. *Prog. Inorg. Chem.* **2003**, *52*, 315−367.
(4) Robertson, N.; Cronin, L. *Coord. Chem. Rev.* **2002**, *227*, 93−127.
(5) Zyss, J., Ed. *Molecular Nonlinear Optics*; Academic Press: Boston, MA, 1993.
(6) Burgmayer, S. J. N. *Prog. Inorg. Chem.* **2003**, *52*, 491−537.
(7) Basu, P.; Stolz, J. F.; Smith, M. T. *Curr. Sci.* **2003**, *84*, 1412−1418.
(8) Hille, R. *Chem. Rev.* **1996**, *96*, 2757−2816.
(9) Zumft, W. G. *Microbiol. Mol. Biol. Rev.* **1997**, *61*, 533−615.
(10) Stolz, J. F.; Basu, P. *ChemBioChem* **2002**, *3*, 198−206.

10.1021/ic051653p CCC: $33.50
Published on Web 03/29/2006

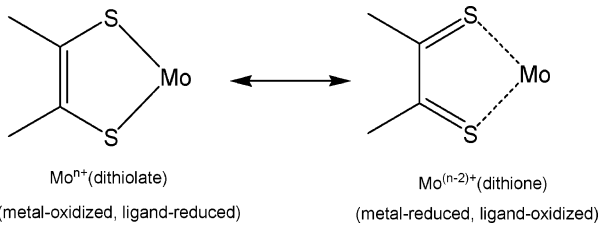

Figure 1. Schematic representation of the metal−ligand redox interplay.

ecules complemented with spectroscopic and reactivity studies.[11−17] A detailed understanding of the influence of the conformational flexibility of the dithiolene ligand on the properties of molybdenum compounds is yet to be fully developed, although the fold angle along the S···S vector has been proposed to modulate the redox behavior of the molybdenum center.[18]

An important approach to understanding the effect of structural flexibilities on the molecular properties is to synthesize well-defined compounds. Recently, molybdenum bis(dithiolate)dicarbonyl compounds have been employed as versatile precursors for the preparation of a variety of molybdenum(IV, V, and VI) complexes.[19,20] We are interested in exploring the chemistry of mono(dithiolate)molybdenum carbonyls for preparation of high-valent molybdenum centers coordinated by one or more dithiolene ligands. Herein, we report the synthesis, characterization, and structure of $(Me_2Pipdt)Mo(CO)_4$ (where Me_2Pipdt = *N*,*N*′-piperazine-2,3-dithione). We chose Me_2Pipdt ligand because of the conformational flexibility of piperazine ring and its "noninnocent" redox properties in different transition-metal complexes.[21−29] The electronic spectra of the $(Me_2Pipdt)Mo(CO)_4$ complex exhibit distinct solvatochromic effects, the details of which have been examined using time-dependent density functional theory (TDDFT) approach coupled with polarized continuum model (PCM) algorithm. A combination of experimental and theoretical approaches was used for investigating the influence of geometric and electronic factors on the solvatochromic properties of a molybdenum dithiooxamidetetracarbonyl complex.

Experimental Section

Preparation of Compound. The synthesis of the molybdenum complex was carried out in an oxygen-free dry argon atmosphere using dry degassed solvents. The ligand, Me_2Pipdt, was synthesized in air. Solvents were purchased either from Aldrich Chemical Co. or Acros Chemical Co. and purified by distillation as follows: acetonitrile from CaH_2, followed by Li_2CO_3−$KMnO_4$ and finally from P_2O_5; CH_2Cl_2 and $CHCl_3$ from CaH_2; toluene from sodium benzophenone; ethanol from sodium ethoxide. $Mo(CO)_6$, *N*,*N*′-dimehylpiperazine-2,3-dione, and Lawesson's reagent were purchased from Aldrich Chemical Co. and used without purification. Silica gel (70−230 mesh) was purchased from Sorbent Technologies.

Synthesis of Me_2Pipdt. This compound was prepared as described in the literature.[30] Yield: 82%. ^{1}H NMR ($CDCl_3$): δ 3.56 (s, 6H, CH_3), 3.74 (s, 4H, CH_2). ^{13}C NMR ($CHCl_3$): δ 45.2 (CH_3), 49.1 (CH_2), 189.0 (C═S). IR (KBr): 2919 (alkyl C−H), 1500 (C═S). UV−vis [λ_{max}, nm (ϵ, M^{-1} cm^{-1}), $CHCl_3$]: 500 (200), 430 (350), 404sh, 360sh, 316 (4300). ESI-MS^- (MeCN): *m*/*z* 174.03, $[M]^-$ calculated for $C_6H_{10}N_2S_2$.

Synthesis of $(Me_2Pipdt)Mo(CO)_4$. A total of 0.50 g (1.8 mol) of $Mo(CO)_6$ was refluxed in 20 mL of acetonitrile for 4 h.[31] To this yellow refluxing solution was added 0.64 g (3.6 mmol) of Me_2Pipdt, and the solution changed to blue instantly. The reaction mixture was allowed to continue refluxing with stirring for 16 h, and then it was cooled to room temperature. During this time, the progress of the reaction was monitored by thin-layer chromatography. Acetonitrile was removed from the reaction mixture under reduced pressure. The resultant dark-blue powder was dissolved in CH_2Cl_2, filtered, and purified by column chromatography on silica gel using 3:1 CH_2Cl_2/hexane as an eluent. The first dark-blue band was collected, and the solvent was evaporated, yielding the target compound. Yield: 34%. ^{1}H NMR (CD_2Cl_2): δ 3.25 (s, 4H, CH_2), 3.31 (s, 6H, CH_3). ^{13}C NMR (CD_2Cl_2): δ 45.68 (CH_2), 50.12 (CH_3), 184.40 (C═S), 202.62 (CO_{ax}), 219.56 (CO_{eq}). IR (KBr): 2962 (w, alkyl C−H), 2932 (w, alkyl C−H), 2865 (w, alkyl C−H), 2009 (s, CO), 1880sh (vs, CO), 1860 (vs, CO), 1838 (vs, CO), 1560 (w), 1510 (s), 1451 (m), 1402 (s), 1354 (vs), 1288 (w), 1267 (m), 1204 (m), 1102 (m), 1039 (w), 1019 (w), 958 (w), 936 (w), 903 (w), 818 (w), 625 (s), 579 (s), 540 (m), 460 (m). UV−vis [λ_{max}, nm (ϵ, M^{-1} cm^{-1}), THF]: 669 (3450), 455sh (378), 383 (746), 310sh (2625), 269 (9980). ESI-MS^- (MeCN): *m*/*z* 419 (60%) [M + Cl]$^-$.

Spectroscopic Measurements. All mass spectra were collected in a Micromass ZMD quadrupole spectrometer equipped with an electrospray ionization (ESI) source in a negative-ion mode, using

(11) Enemark, J. H.; Young, C. G. *Adv. Inorg. Chem.* **1993**, *40*, 1−88.
(12) Enemark, J. H.; Cooney, J. J. A.; Wang, J.-J.; Holm, R. H. *Chem. Rev.* **2004**, *104*, 1175−1200.
(13) Young, C. G.; Wedd, A. G. *Chem. Commun.* **1997**, 1251−1257.
(14) Nemykin, V. N.; Basu, P. *Dalton Trans.* **2004**, 1928−1933.
(15) Nemykin, V. N.; Laskin, J.; Basu, P. *J. Am. Chem. Soc.* **2004**, *126*, 8604−8605.
(16) McMaster, J.; Tunney, J. M.; Garner, C. D. *Prog. Inorg. Chem.* **2003**, *52*, 539−583.
(17) Snyder, B. S.; Rao, C. P.; Holm, R. H. *Aust. J. Chem.* **1986**, *39*, 963−74.
(18) Joshi, H. K.; Cooney, J. A.; Inscore, F. E.; Gruhn, N. E.; Lichtenberger, D. L.; Enemark, J. H. *Proc. Natl. Acad. Sci., USA* **2003**, *100*, 3719−3724. Joshi, H. K.; Enemark, J. H. *J. Am. Chem. Soc.* **2004**, *126*, 11784−11785.
(19) Fomichev, D. V.; Lim, B. S.; Holm, R. H. *Inorg. Chem.* **2001**, *40*, 645−654.
(20) Lim, B. S.; Donahue, J. P.; Holm, R. H. *Inorg. Chem.* **2000**, *39*, 263−273.
(21) Cau, L.; Deplano, L.; Marchió, L.; Mercuri, M. L.; Pilia, L.; Serpe, A.; Trogu, E. F. *Dalton Trans.* **2003**, 1969−1974.
(22) Deplano, P.; Mercuri, M. L.; Marchió, L.; Pilia, L.; Salidi, M.; Serpe, A.; Tronki, E. *Inorg. Chim. Acta* **2004**, *357*, 1608−1612.
(23) Bigoli, F.; Deplano, P.; Mercuri, M. L.; Pellinghelli, M. A.; Pilia, L.; Pintus, G.; Serpe, A.; Trogu, E. F. *Inorg. Chem.* **2002**, *41*, 5241−5248.
(24) Bigoli, F.; Chen, C.-T.; Wu, W.-C.; Deplano, P.; Mercuri, M. L.; Pellinghelli, M. A.; Pilia, L.; Pintus, G.; Serpe, A.; Trogu, E. F. *Chem. Commun.* **2001**, 2246−2247.
(25) Servaas, P. C.; Stufkens, D. J.; Oskam, A.; Vernooijs, P.; Baerends, E. J.; De Ridder, D. J. A.; Stam, C. H. *Inorg. Chem.* **1989**, *28*, 4104−4113.
(26) Dieck, H. T.; Form, M. *Z. Anorg. Allg. Chem.* **1984**, *515*, 19−35.
(27) Dieck, H. T.; Hohmann, F.; Form, M.; Mack, T.; Renk, I. W. *J. Less-Common Met.* **1977**, *54*, 221−231.
(28) Green, M. R.; Jubran, N.; Bursten, B. E.; Busch, D. H. *Inorg. Chem.* **1987**, *26*, 2326−2332.
(29) Hohmann, F.; Dieck, H. T. *J. Organomet. Chem.* **1976**, *122*, 197−208.
(30) Isaksson, R.; Liljefors, T.; Sandstorm, J. *J. Chem. Res., Synop.* **1981**, 43.
(31) Tate, D. P.; Knipple, W. R.; Augl, J. M. *Inorg. Chem.* **1962**, *1*, 433−434. Baker, P. K. *Chem. Soc. Rev.* **1998**, *27*, 125−132 and references cited therein. Baker, P.; Drew, M. G. B.; Meehan, M. M.; Parker, E. E. *J. Chem. Crystallogr*. **2003**, *33*, 669−672.

Table 1. Crystallographic Data on the (Me$_2$Pipdt)Mo(CO)$_4$ Complex

formula	$C_{10}H_{10}Mo_1N_2O_4S_2$
cryst syst	monoclinic
space group	$P2_1/n$
cell param	
a, Å	25.541(3)
b, Å	10.3936(14)
c, Å	10.9012(12)
β, deg	92.261(9)
V, Å^3	2891.6(6)
Z	8
radiation type	Mo Kα
cryst size	0.05 mm × 0.40 mm × 0.45 mm
reflns measd	7016
indep reflns	6644
reflns used $\sigma \geq 4.00$	3390
R_f	0.033
R_w	0.057
no. of param	343
GOF	0.905

acetonitrile as the mobile phase. The nebulizer tip was set at 3.5 kV and 80 °C, and dry nitrogen was used as the bath gas. UV−visible spectra were recorded on a modified temperature-controlled Cary 14 spectrophotometer with OLIS 14 version 2.6.99 operating system. ^{1}H and ^{13}C NMR data were collected using a Bruker ACP-300 spectrometer. IR spectra were recorded on a Perkin-Elmer FT-IR 1760X spectrometer in KBr pellets.

X-ray Structure Determination. Crystals of (Me$_2$Pipdt)Mo(CO)$_4$ were obtained by slow diffusion of hexane into saturated CH_2Cl_2, $CHCl_3$, or toluene solutions of the crude compound at 4 °C inside an inert-atmosphere drybox. This approach provided well-shaped dark-blue X-ray-quality single crystals. Intensity data were collected using a Rigaku AFC-7R diffractometer at room temperature with Mo Kα radiation and a graphite monochromator. A total of 7016 reflections were collected ($\theta = 2.5-27.5°$); of these, 6644 reflections were unique {$R_{int} = 0.017$ [$I > 3\sigma(I)$]}. The data were corrected for absorption using the ψ-scan method. All raw data were processed using the TeXsan 10.3b program.[32] The structure was solved by the Patterson method and refined by full-matrix least-squares procedures on F^2 using the Crystals for Windows program.[33] The three-parameter Prince-modified Chebychev polynomial weighting scheme incorporated in the program was used for the refinement. All non-hydrogen atoms were refined anisotropically, while the hydrogen atoms were found in calculated positions and refined by the riding model. Important crystallographic data are presented in Table 1.

Computational Details. All computations were performed using the *Gaussian 03*[34] software package running under Windows or UNIX OS. Gas- and solution-phase geometries were obtained by optimizing the geometry obtained from the crystal structure without any symmetry constraints. The solution-phase geometries of (Me$_2$Pipdt)Mo(CO)$_4$ in toluene and acetonitrile were calculated using a PCM algorithm implemented in the *Gaussian 03* program.[35] In all cases, vibrational frequencies were calculated to ensure that optimized geometries represented local minima. The excitation energies were calculated by the TDDFT approach. Calculations in solutions were performed using both equilibrium and nonequilibrium versions of the PCM module, and in all cases, the lowest 40 singlet excited states were considered. In addition, the NMR properties of the dithiooxamide ligand and (Me$_2$Pipdt)Mo(CO)$_4$ complex were calculated using the GIAO algorithm[36] incorporated in the *Gaussian 03* program. The NMR shifts were calculated as the difference between magnetic shielding of the atom of interest and that in the reference molecule (tetramethylsilane) optimized at the same level of theory. In all calculations, Becke's three-parameter hybrid exchange functional[37] and the Lee−Yang−Parr nonlocal correlation functional[38] (B3LYP) were used. The full-electron DZVP[39] basis set was used for molybdenum, while for all other atoms, the 6-311G(d)[40] basis set was employed. This combination of the exchange-correlation functional and basis set, reported recently for a number of molybdenum complexes, resulted in vertical excitation energies in good agreement with the experiment.[41−43] The percentage of atomic orbital contributions to their respective molecular orbitals was calculated by using the *VMOdes* program.[44]

Results and Discussion

1. Synthesis and Molecular Structure of (Me$_2$Pipdt)Mo(CO)$_4$. Molecules of the general formula $X_2Mo(CO)_4$ can be synthesized through a ligand-exchange reaction of activated tetracarbonyl precursors (Figure 2). Examples of such precursors include (norbornadiene)Mo(CO)$_4$, (PPh$_3$O)$_2$Mo(CO)$_4$, (piperidine)$_2$Mo(CO)$_4$, (CH$_3$CN)$_2$Mo(CO)$_4$, and Mo(CO)$_5$X. Weakly coordinated molybdenum complexes are usually isolated prior to the exchange reaction.[26,27,45−48] Although in acetonitrile Mo(CO)$_6$ forms a variety of (CH$_3$CN)$_n$Mo(CO)$_{6-n}$ compounds,[31] it proved unnecessary to isolate these precursor compounds prior to reaction with the Me$_2$Pipdt ligand. In the reaction mixture, no (Me$_2$Pipdt)Mo(CO)$_3$(CH$_3$CN) or (Me$_2$Pipdt)$_2$Mo(CO)$_2$ compound was

(32) TeXsan 10.3.b; Rigaku Inc.: Tokyo, Japan, 1998.
(33) Betteridge, P. W.; Carruthers, J. R.; Cooper, R. I.; Prout, K.; Watkin, D. J. *J. Appl. Crystallogr.* **2003**, *36*, 1487.
(34) Frisch, M. J.; Trucks, G. W.; Schlegel, H. B.; Gill, P. M. W.; Johnson, B. G.; Robb, M. A.; Cheeseman, J. R.; Keith, T. A.; Petersson, G. A.; Montgomery, J. A.; Raghavachari, K.; Al-Laham, M. A.; Zakrzewski, V. G.; Ortiz, J. V.; Foresman, J. B.; Cioslowski, J.; Stefanov, B. B.; Nanayakkara, A.; Challacombe, M.; Peng, C. Y.; Ayala, P. Y.; Chen, W.; Wong, M. W.; Andres, J. L.; Replogle, E. S.; Gomperts, R.; Martin, R. L.; Fox, D. J.; Binkley, J. S.; Defrees, D. J.; Baker, J.; Stewart, J. P.; Head-Gordon, M.; Gonzalez, C.; Pople, J. A. *Gaussian 98*; Gaussian, Inc.: Pittsburgh, PA, 1998.
(35) Miertus, S.; Scrocco, E.; Tomasi, J. *Chem. Phys.* **1981**, *55*, 117−129.
(36) Wolinski, K.; Hinton, J. F.; Pulay, P. *J. Am. Chem. Soc.* **1990**, *112*, 8251−8260.
(37) Becke, A. D. *Phys. Rev. A* **1988**, *38*, 3098−3100.
(38) Lee, C.; Yang, W.; Parr, R. G. *Phys. Rev. B* **1988**, *37*, 785−789.
(39) Basis sets were obtained from the Extensible Computational Chemistry Environment Basis Set Database, version 4/22/01, as developed and distributed by the Molecular Science Computing Facility, Environmental and Molecular Sciences Laboratory, which is part of the Pacific Northwest Laboratory, P.O. Box 999, Richland, WA 99352, and funded by the U.S. Department of Energy. The Pacific Northwest Laboratory is a multiprogram laboratory operated by Battelle Memorial Institute for the U.S. Department of Energy under Contract DE-AC06-76RLO 1830. Contact David Feller or Karen Schuchardt for further information.
(40) McLean, A. D.; Chandler, G. S. *J. Chem. Phys.* **1980**, *72*, 5639−5948. Krishnan, R.; Binkley, J. S.; Seeger, R.; Pople, J. A. *J. Chem. Phys.* **1980**, *72*, 650−654.
(41) Nemykin, V. N.; Basu, P. *Inorg. Chem.* **2003**, *42*, 4046−4056.
(42) Basu, P.; Nemykin, V. N.; Sengar, R. S. *Inorg. Chem.* **2003**, *42*, 7489−7501.
(43) McNaughton, R. L.; Mondal, S.; Nemykin, V. N.; Basu, P.; Kirk, M. L. *Inorg. Chem.* **2005**, *44*, 8216−8222.
(44) Nemykin, V. N.; Basu, P. *VMOdes: Virtual Molecular Orbital description program for Gaussian, GAMESS, and HyperChem*, revision A7.1; 2003.
(45) Sellman, D.; Zapf, L. *J. Organomet. Chem.* **1985**, *289*, 57−69.
(46) Abel, E. W.; Moss, I.; Orrell, K. G.; Šik, V. *J. Organomet. Chem.* **1987**, *326*, 187−200.
(47) Barton, A. J.; Levason, W.; Reid, G. *J. Organomet. Chem.* **1999**, *579*, 235−242.
(48) Myrex, R. D.; Colbert, C. S.; Gray, G. M. *Organometallics* **2004**, *23*, 409−415.

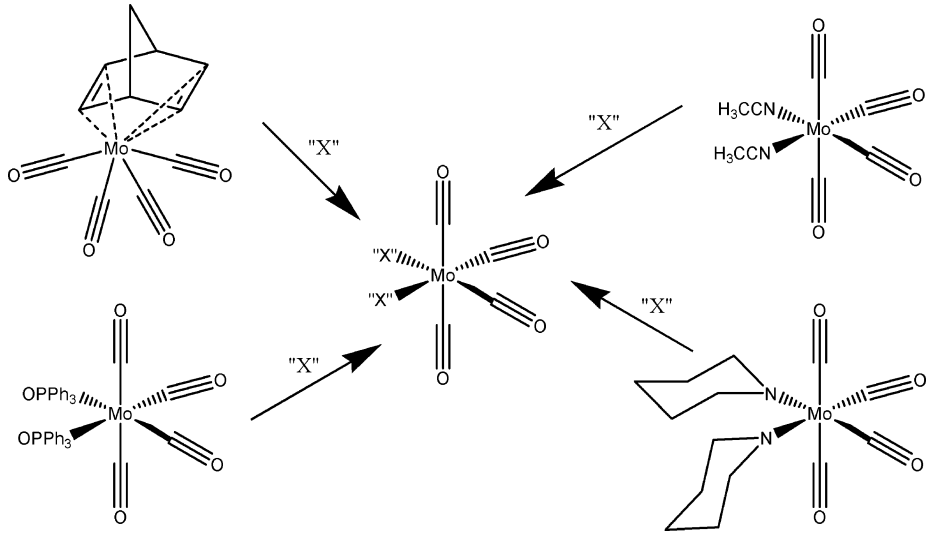

Figure 2. Representative strategies for synthesizing molybdenum tetracarbonyl compounds.

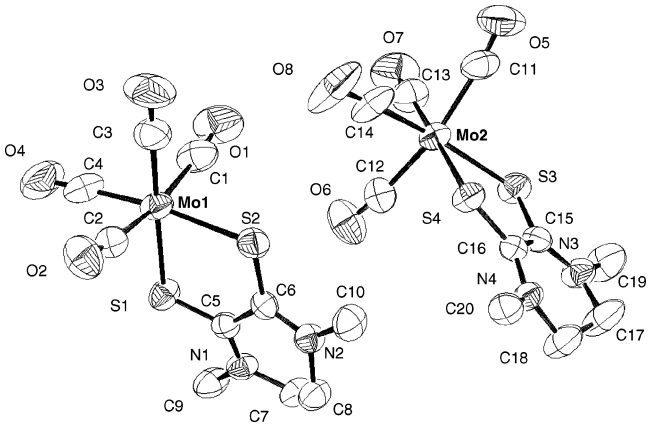

Figure 3. CAMERON plot of two independent molecules of the $(Me_2Pipdt)Mo(CO)_4$ complex with 50% probability ellipsoids.

Table 2. Selected Bond Distances (Å) and Angles (deg) for $(Me_2Pipdt)Mo(CO)_4$

molecule 1		molecule 2	
Mo1−C1	2.043(7)	Mo2−C11	2.019(6)
Mo1−C2	2.018(6)	Mo2−C12	2.029(6)
Mo1−C3	1.963(6)	Mo2−C13	1.965(7)
Mo1−C4	1.966(7)	Mo2−C14	1.946(7)
Mo1−S1	2.522(2)	Mo2−S3	2.525(2)
Mo1−S2	2.520(2)	Mo2−S4	2.520(2)
C5−S1	1.680(5)	C15−S3	1.674(5)
C6−S2	1.668(5)	C16−S4	1.681(5)
C6−C5	1.493(6)	C16−C15	1.495(7)
C5−N1	1.328(6)	C15−N3	1.334(6)
C6−N2	1.336(6)	C16−N4	1.321(5)
S1−Mo1−S2	79.70(5)	S3−Mo2−S4	79.08(5)
C3−Mo1−C4	90.8(3)	C14−Mo2−C13	91.1(3)
C1−Mo1−C2	167.4(2)	C11−Mo2−C12	167.7(2)
S2−Mo1−C4	170.93(18)	S3−Mo2−C14	169.26(18)
S1−Mo1−C3	177.9(2)	S4−Mo2−C13	177.67(19)

detected by ESI-MS, although $Mo(CO)_6$ forms $Mo(CH_3CN)_3(CO)_3$ and $Mo(CH_3CN)_4(CO)_2$ in acetonitrile. $(Me_2Pipdt)Mo(CO)_4$ is soluble in common organic solvents but insoluble in water. While in the solid state the deep-blue $(Me_2Pipdt)Mo(CO)_4$ is air-stable, in solution it decomposes. Qualitatively, the stability follows the order aromatic hydrocarbons > chlorinated hydrocarbons > aprotic polar solvents > alcohols.

The molecular structure of $(Me_2Pipdt)Mo(CO)_4$ has been determined by single-crystal X-ray diffractometry. The CAMERON diagram of $(Me_2Pipdt)Mo(CO)_4$ is presented in Figure 3, while selected metric parameters are listed in Table 2. Three-dimensional solid-state crystal structures of the molybdenum tetracarbonyldithiolate or -dithione complexes are rare.[49] Indeed, $(Me_2Pipdt)Mo(CO)_4$ is only the second example of a mononuclear system where the $Mo(CO)_4$ fragment coordinated to a dithione or dithiolate ligand and the first example of a cyclic dithiooxamide ligand coordinated to a $Mo(CO)_4$ fragment. The unit cell consists of eight molecules, with two of them being unique. The bond distances and angles of the two unique molecules present in the unit cell are almost invariant; however, the torsion angles are slightly different (1−2°). The complex possesses a pseudooctahedral geometry with two equatorial and two axial carbonyl ligands. The observed Mo−C distances are typical for molybdenum carbonyl complexes, with equatorial bonds being shorter because of the smaller trans effect of the dithiooxamide ligand. The $C_{eq}-Mo-C_{eq}$ angle is ca. 90°, while $C_{ax}-Mo-C_{ax}$ deviates significantly from 180° (Table 2) perhaps because of electronic repulsion between occupied out-of-plane atomic orbitals of sulfur atoms and π orbitals of axial carbonyl ligands. A similar bending of the axial carbonyl ligands has been observed in $X_2Mo(CO)_4$ complexes where molybdenum is coordinated by a sulfur donor.[50−53]

The possible active redox behavior of the dithiolate ligand in a variety of transition-metal compounds, including molybdoenzymes, has been discussed in the literature.[12,13,19] For example, in complexes of the general formula $(R_4N_2C_2S_2)$-

(49) CCDC database, V5.26, Cambridge, U.K., Nov 2004.

(50) Gormley, F. K.; Gronbach, J.; Draper, S. M.; Davis, A. P. *J. Chem. Soc., Dalton Trans.* **2000**, 173−179.
(51) Yih, K.-H.; Lee, G.-H.; Wang, Y. *J. Organomet. Chem.* **2003**, *665*, 114−121.
(52) Yih, K.-H.; Lee, G.-H.; Wang, Y. *J. Organomet. Chem.* **1999**, *588*, 125−133.
(53) Sellmann, D.; Binker, G.; Schwarz, J.; Huttner, G.; Zsolnai, L. *J. Organomet. Chem.* **1987**, *323*, 323−338.

Table 3. Comparison of NC(S)C(S)N Torsion Angles (θ) in Me$_2$Pipdt and (Me$_2$Pipdt)$_n$ML$_x$ Compounds

structure	θ, deg	ref
Me$_2$Pipdt	35.4	54
Me$_2$PipdtI$_3$	6.88	57
[(Me$_2$Pipdt)$_2$Pt][Pt(mnt)$_2$]	12.7	22
(Me$_2$Pipdt)Re(CO)$_3$Br	18.0	24
[(Me$_2$Pipdt)$_2$Ni][BF$_4$]	7.71	23
(Me$_2$Pipdt)Ni(mnt)	0.83	23
[(Me$_2$Pipdt)$_2$Pt][I$_3$]$_2$	10.2	57
[Cu(Bzl$_2$DTO)$_2$][ClO$_4$]$_2$	36.3	56
Zn(Me$_2$DTO)Cl$_2$	36.9	56
(Me$_2$Pipdt)Mo(CO)$_4$ (**1**)	11.2	this work
(Me$_2$Pipdt)Mo(CO)$_4$ (**2**)	12.9	this work

Mo(CO)$_4$, the molybdenum atom has an oxidation state of 0 and the ligand is viewed as a dithione, while in complexes of the general formula (R$_4$N$_2$C$_2$S$_2$)Mo(CO)$_2$(PR$_3$)$_2$, the same ligand is viewed as a dithiolate and the oxidation state of the molybdenum is 2+.[26,27,54] In the latter case, the dithiolate nature of the ligand is suggested because of a short carbon−carbon (1.364 Å) bond in the NC(S)C(S)N fragment and the planar metal-containing chelate ring.[54] In (Me$_2$Pipdt)Mo(CO)$_4$, the Mo−S distance (2.52 Å) is longer than the typical Mo−S distance of 2.36−2.46 Å observed in numerous dithiolatemolybdenum complexes, which suggests the presence of a Mo−S(thione) coordination and a zerovalent metal.[12,19,20,55] On the other hand, the observed C−C and C−S distances are ∼0.04 and 0.01 Å shorter, respectively, as compared to the free ligand.[56] Moreover, the observed dihedral angle (11.2−12.9°) between the planes comprising the two thioamide groups in (Me$_2$Pipdt)Mo(CO)$_4$ is significantly smaller than that in the free ligand and its copper, rhenium, and zinc complexes (Table 3).[25,57] The shorter distances imply a small contribution of the dithiolate form to the structure of (Me$_2$Pipdt)Mo(CO)$_4$. In many cases, the NC(S)C(S)N dihedral angles in the free Me$_2$Pipdt ligand reduce dramatically when the ligand is oxidized or coordinates to a metal ion (Table 3).[22−24,58] Thus, deriving the oxidation states using metric parameters only is not a straightforward process, although it has been successfully applied for ((C$_5$H$_{10}$N)$_2$C$_2$S$_2$)Mo(CO)$_2$(PBu$_3$)$_2$.[54]

The flexibility of the dihedral angle in the Me$_2$Pipdt ligand was further probed by DFT calculations. The metric parameters in the optimized geometry of the free Me$_2$Pipdt are in excellent agreement with the X-ray structure (Table S1 in the Supporting Information). The geometry of the molybdenum complex (Me$_2$Pipdt)Mo(CO)$_4$ was optimized in both the gas and solution phases (Figure 4 and Table 4). Figure 4 clearly suggests the flexibility of the NC(S)C(S)N dihedral angle: 1.05° in the gas phase, 5.44° in toluene, and 11.99° in acetonitrile. The latter is very close to that observed in the solid state (Table 4). The gas-phase DFT calculations predict the bond distances and the important angles, with the maximum deviation of 0.05 Å and 2.3° for the distances and angles, respectively. With increasing polarity of the solvent, the Mo−S distances increase significantly, Mo−CO(eq) bonds reduce slightly, and Mo−CO(ax) bond distances remain the same. In addition, the C(ax)−Mo−C(ax) angle changes from 169.4° in the gas phase to 174.1° in acetonitrile, while the C(eq)−Mo−C(eq) angle decreases from 93.31 to 90.98°. Interestingly, the C═S and C−C bond distances in the MoS2C2 chelate ring remain the same, indicating that the dithiooxamide form of the Me$_2$Pipdt ligand is unchanged in the solid state, gas phase, and solution phase. Overall, the increase of the solvent polarity primarily affects the Mo−S distance, the C(ax)−Mo−C(ax) angle, and the NC(S)C(S)N dihedral angle. The flexibility of the N(S)CC(S)N torsion angle leads to questions such as the following: Do the dihedral angles found in the solid state agree with those in the solution phase? Can this angle modulate the overlap between the molybdenum d orbitals and sulfur p orbitals?

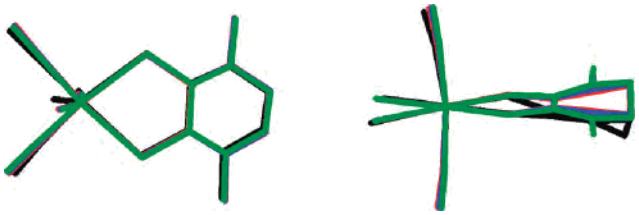

Figure 4. Superimposition of the molecular structures of the (Me$_2$Pipdt)Mo(CO)$_4$ complex from crystallography and calculation: black, X-ray; red, in a vacuum; blue, in toluene; olive, in acetonitrile.

Table 4. Comparison between Calculated and Experimental Bond Distances and Angles for the (Me$_2$Pipdt)Mo(CO)$_4$ Complex[a]

	X-ray molecule **1**	X-ray molecule **2**	gas-phase DFT	toluene DFT	acetonitrile DFT
Mo−C(ax)	2.024	2.030	2.079	2.076	2.072
Mo−C(eq)	1.956	1.964	2.011	2.004	1.991
C−O(ax)	1.146	1.143	1.144	1.148	1.149
C−O(eq)	1.154	1.150	1.153	1.156	1.161
Mo−S	2.522	2.521	2.544	2.567	2.596
S−C	1.677	1.674	1.691	1.693	1.697
C(ax)−Mo−C(ax)	167.69	167.37	169.42	171.6	174.1
C(eq)−Mo−C(eq)	91.07	90.74	93.31	92.12	90.98
S−Mo−S	79.08	79.70	78.62	78.41	78.33
NC(S)C(S)N	11.2	12.9	1.05	5.4	12.0

[a] The average parameters are given for the crystal structure.

2. Spectroscopy of Me$_2$Pipdt and (Me$_2$Pipdt)Mo(CO)$_4$. The room-temperature ^{1}H NMR spectrum of (Me$_2$Pipdt)Mo(CO)$_4$ exhibits resonances due to the methyl and methylene groups in their usual positions with no observable change due to the conformational flexibility of the piperazine ring.[46,47,54] The ^{13}C{^{1}H} NMR spectra of the free ligand and the complex show little shift in the methylene and methyl carbons, with the largest difference being 1 ppm. In addition, the C═S resonances in the free ligand (189.0 ppm) and in (Me$_2$Pipdt)Mo(CO)$_4$ (184.4 ppm) differ by 4.6 ppm. In contrast, the C(S) carbons in (Et$_4$N$_2$C$_2$S$_2$)Mo(PPh$_3$)$_2$(CO)$_2$ resonate at 162.75 ppm, ∼30 ppm downfield from the free Et$_4$N$_2$C$_2$S$_2$ ligand (193.02 ppm), clearly indicating the

(54) Barnard, K. R.; Wedd, A. G.; Tiekink, E. R. *Inorg. Chem.* **1990**, *29*, 891−892.
(55) Beswick, C. L.; Schulman, J. M.; Stiefel, E. I. *Prog. Inorg. Chem.* **2003**, *52*, 55−110.
(56) De Ridder, D. J. A. *Acta Crystallogr.* **1993**, *C49*, 1975−1976.
(57) Antolini, L.; Fabretti, A. C.; Franchini, G.; Menabue, L.; Pellacani, G. C.; Desseyn, H. O.; Dommisse, R.; Hofmans, H. C. *J. Chem. Soc., Dalton Trans.* **1987**, 1921−1928.
(58) Bigoli, F.; Deplano, P.; Mercuri, M. L.; Pellinghelli, M. A.; Pintus, G.; Serpe, A.; Trogu, E. F. *J. Am. Chem. Soc.* **2001**, *123*, 1788−1789.

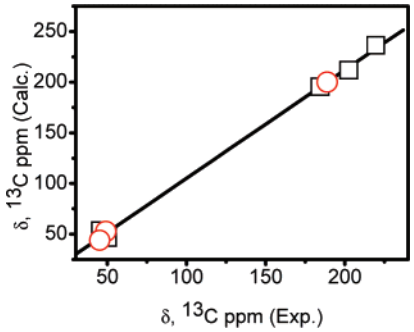

Figure 5. Linear correlation between the experimental and calculated ^{13}C NMR chemical shifts of Me_2Pipdt (circles) and $(Me_2Pipdt)Mo(CO)_4$ (squares). δ (ppm, calcd) $1.07 \times \delta$ (ppm, exptl) $- 1.90$.

transformation of the dithione into the dithiolate form.[54] Thus, $^{13}C\{^1H\}$ NMR data on $(Me_2Pipdt)Mo(CO)_4$ suggest that the sulfur-containing ligand remains in the dithione form.

The ^{13}C NMR chemical shifts for the axial carbonyl groups (202.6 ppm) are similar to those observed in $Mo(CO)_6$ (203.4 ppm),[59] indicating marginal electronic interactions between the axial and equatorial ligands. The chemical shift for the equatorial carbonyl ligands (219.6 ppm) reflects poorer σ-donor and stronger π-acceptor properties of the sulfur atoms that are responsible for withdrawal of the electron density from the equatorial carbonyl group. The observed difference between the chemical shifts in the axial and equatorial carbonyl groups (17 ppm) is typical for $X_2Mo(CO)_4$ complexes reported in the literature.[46,47] Our experimental observations and assignments were further complimented by GIAO DFT calculations, and the calculated chemical shifts for Me_2Pipdt and $(Me_2Pipdt)Mo(CO)_4$ agree well with the experimental data (Figure 5).

In complexes of the general formula $X_2Mo(CO)_4$ with effective C_{2v} symmetry, four carbonyl ligand vibrations with A_1 (two vibrations) and B_2 (two vibrations) symmetries are expected to be observed in the IR spectra.[26,46−48] The observed carbonyl frequencies in $(Me_2Pipdt)Mo(CO)_4$ [2009, 1880, 1860 (sh), and 1838 cm^{-1}] are close to those published for $(i\text{-}Pr_2Pipdt)Mo(CO)_4$ (2015, 1880, 1863, and 1810 cm^{-1}).[26] The DFT calculations (Figure S1 and Table S2 in the Supporting Information) predict three carbonyl vibrations within a narrow area of the IR spectrum. The first and second carbonyl bands are separated by 22 cm^{-1} (calculated as 26 cm^{-1}), while the separation between the second and third bands is smaller (10 and 7 cm^{-1} for the experimental and calculated frequencies, respectively). The calculations also suggest that the fourth carbonyl band should be well-separated from the other three in excellent agreement with the experimental observations. While the difference in the calculated frequencies matches well the experiment, the absolute values of the frequencies are lower than the experimental values, which reflect a general tendency of the DFT approach to underestimate the vibrational energies and are typically adjusted by using different scaling factors.[60]

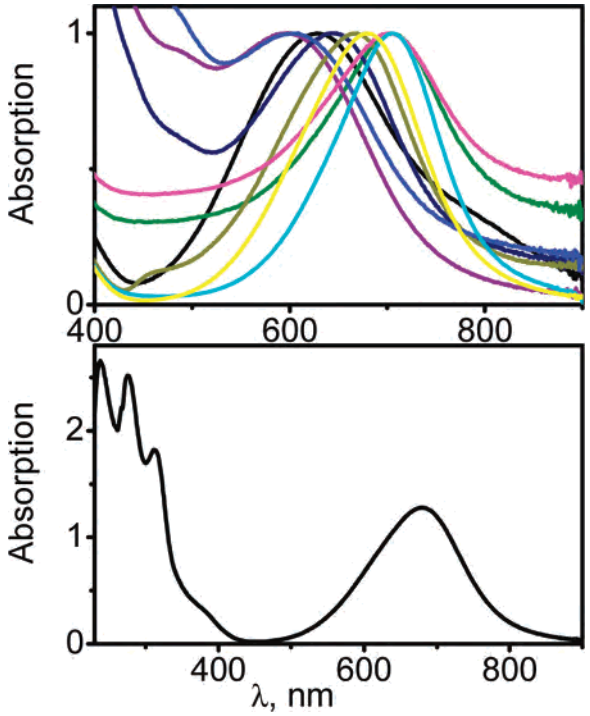

Figure 6. Top: UV−visible spectrum of $(Me_2Pipdt)Mo(CO)_4$ in dichloromethane. Bottom: λ_{max} (nm) as a function of solvent (black, acetonitrile, 628; blue, DMF, 609; magenta, $CHCl_3$, 701; dark yellow, THF, 669; navy, pyridine, 645; purple, DMSO, 596; olive, benzene, 705; cyan, toluene, 704; yellow, CH_2Cl_2, 678).

Negative-ion ESI-MS spectra of $(Me_2Pipdt)Mo(CO)_4$ at low cone voltages show a peak cluster due to the $[M + Cl]^-$ ion, while the intensity of the $[M]^-$ peak was found to be negligibly small (Figure S2 in the Supporting Information). The formation of the $[M + Cl]^-$ ion is not surprising because it provides a common ionization pathway in the negative mode of ESI-MS experiments,[61] although such an ionization pathway is not characteristic for transition-metal carbonyls, where often chemical derivatization by alkoxide ions is necessary.[62,63] In our case, the $[M + Cl]^-$ but not the $[M + OMe]^-$ ion is observed even in the presence of methoxide ions, which indicates a high electron density at the molybdenum center and lower electrophilicity of the CO ligands. A peak cluster due to the $[M + Cl - 2CO]^-$ ion has been observed as the primary daughter ion originating from $(Me_2Pipdt)Mo(CO)_4$, while a peak cluster due to $[M + Cl - CO]^-$ of smaller intensity has also been observed. Upon an increase in the cone voltage (i.e., collision energy), peaks due to $[M + Cl - 3CO]^-$ and $[M + Cl - 4CO]^-$ have also been observed, suggesting a stepwise dissociation of the carbonyl ligand(s) and a stronger binding of the Me_2Pipdt ligand to the molybdenum center as compared to the carbonyl ligands.

The electronic spectra of $(Me_2Pipdt)Mo(CO)_4$ have been investigated in a variety of solvents and exhibit high-intensity bands in the visible area and several bands in the UV region (Figure 6 and Table S3 in the Supporting Information). One

(59) Bach, C.; Willner, H.; Wang, C.; Rettig, S. J.; Trotter, J.; Aubke, F. *Angew. Chem., Int. Ed. Engl.* **1996**, *35*, 1974−1976.
(60) Foresman, J. B.; Frisch, A. *Exploring chemistry with electronic structure methods*, 2nd ed.; Gaussian Inc.: Pittsburgh, PA, 1996.
(61) Cole, R. B., Ed. *Electrospray Ionization Mass Spectrometry: Fundamentals, Instrumentation, and Applications*; Wiley: New York, 1997; p 570.
(62) Henderson, W.; McIndoe, J. S.; Nicholson, B. K.; Dyson, P. J. *J. Chem. Soc., Dalton Trans.* **1998**, 519−525.
(63) Nemykin, V. N.; Basu, P. *Inorg. Chim. Acta* **2005**, *358*, 2876−2882.

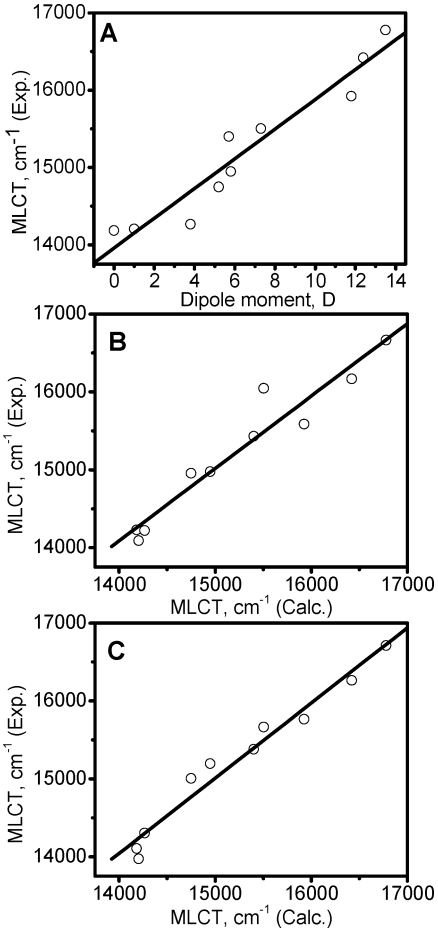

Figure 7. (A) Correlation between the energy of the MLCT band and the dipole moment (μ) of the solvent ($E = 192.265\mu + 13959.04$). (B) Correlation between the experimental and calculated (eq 2; see text) energies of the MLCT band ($E = 200.817\alpha + 1774.779\beta + 3133.748\pi^* + 12184.527$). (C) Correlation between the experimental and calculated (eq 1; see text) energies of the MLCT bands [$E = -26.806\alpha + 1405.203\beta + 2911.175(\pi^* - 501.148\delta) + 466.242$].

of the most interesting features of (Me$_2$Pipdt)Mo(CO)$_4$ is that the low-energy band has been found to be strongly dependent on the solvent polarity: the higher the polarity, the higher is the transition energy (i.e., negative solvatochromism), with the maximum shift being of 2594 cm^{-1}. In the solid state, the complex is deep blue, and the solution color changes depending on the solvent. It is deep blue in pyridine and acetonitrile, navy blue in tetrahydrofuran (THF) and dichloromethane (DCM), violet-blue in dimethylformamide (DMF) and dimethyl sulfoxide (DMSO), and blue-green in benzene, toluene, and chloroform.

The energy of the color-defining band near 650 nm linearly correlates with the dipole moment of the solvents (Figures 7 and S3 in the Supporting Information).[64] The band position can also be related with the Kamlet−Taft model (eqs 1 and 2),[65] where E^0, s, d, a, and b are the coefficients determined

$$E\ (\mathrm{cm}^{-1}) = E^0 + s(\pi^* + d\delta) + a\alpha + b\beta \qquad (1)$$

$$E\ (\mathrm{cm}^{-1}) = E^0 + s\pi^* + a\alpha + b\beta \qquad (2)$$

from regression analysis, α is the hydrogen-bond-donation ability of the solvent, while β is the hydrogen-bond-acceptance ability of the solvent; π^* is a parameter that describes the dipolarity and polarizability of the solvent, and the δ term is dependent on the class of the solvent to be studied. Often the contribution from the last term is negligibly small, which led to the modified Kamlet−Taft expression shown in eq 2. These two equations when correlated with the experimental data led to correlation coefficients $r^2 = 0.98$ and 0.96 for eqs 1 and 2, respectively. Because of the limited number of solvents and the large number of parameters used, however, these correlations should be used with caution.

3. Electronic Structure and Solvatochromic Effect Calculations. Tentatively, the low-energy band observed in (dithiooxamide)Mo(CO)$_4$ complexes has been assigned as the metal-to-ligand charge-transfer (MLCT) transition.[26,27] To understand the nature of the observed UV−visible transitions and to explain the solvatochromic properties of (Me$_2$Pipdt)Mo(CO)$_4$, a series of DFT, TDDFT, and TDDFT-PCM calculations have been conducted.

First, we will discuss the electronic structure of Me$_2$Pipdt and (Me$_2$Pipdt)Mo(CO)$_4$. The results of the electronic structure calculations on the Me$_2$Pipdt ligand are presented in Figure S4 in the Supporting Information, while the compositions of selected molecular orbitals are listed in Table S4 in the Supporting Information. The electronic structures of (Me$_2$Pipdt)Mo(CO)$_4$ calculated by DFT methods are presented in Figure 8, while the compositions of selected molecular orbitals are listed in Table 5. For Me$_2$Pipdt, the frontier orbitals have large contributions from the sulfur atoms. For instance, the two highest occupied molecular orbitals (HOMOs) consist of 74% sulfur π orbitals. The next two lower energy orbitals predominantly consist of sulfur out-of-plane π orbitals with significant contributions from the thiocarbonyl carbon and the nitrogen atoms. These four frontier occupied orbitals are energetically well-separated from the other occupied molecular orbitals. The lowest unoccupied molecular orbital (LUMO) is mostly localized on the C═S fragment and predominantly out-of-plane π orbitals. Again, this orbital is energetically well-separated from the LUMO+1 orbital, which has a large contribution from sulfur out-of-plane π orbitals. Next, several virtual orbitals (LUMO+2 to LUMO+8) are primarily located on carbon and nitrogen atoms and are not expected to contribute to the coordination properties of the ligand. Thus, the frontier molecular orbitals in the Me$_2$Pipdt ligand indicate that the most possible mechanism for the ligand−metal interaction involves in-plane and out-of-plane orbitals of sulfur atoms

(64) We correlated the experimentally observed energy of the low-energy band in the (Me$_2$Pipdt)Mo(CO)$_4$ complex with various empirical solvent parameters as well as experimentally derived constants. The solvent scales such as Kosower's Z (Kosover, E. *J. Am. Chem. Soc.* **1958**, *80*, 3253−3260), Reichard's E*MLCT (Reichardt, C. *Angew. Chem., Int. Ed. Engl.* **1965**, *4*, 29−39), normalized E*MLCT (Reichardt, C. *Solvents and solvent effects in organic chemistry*, 2nd ed.; Wiley-VCH: Weinheim, Germany, 1988), Gutmann's AN and DN (Marcus, Y. *Chem. Soc. Rev.* **1993**, 409−416), and Eisenberg's empirical Pt(NN)(SS) (Cummings, S. D.; Eisenberg, R. *J. Am. Chem. Soc.* **1996**, *118*, 1949−1960) gave considerably weak correlations.

(65) Kamlet, M. J.; Abboud, J.-L. M.; Taft, R. W. *J. Am. Chem. Soc.* **1977**, *99*, 6027−6038.

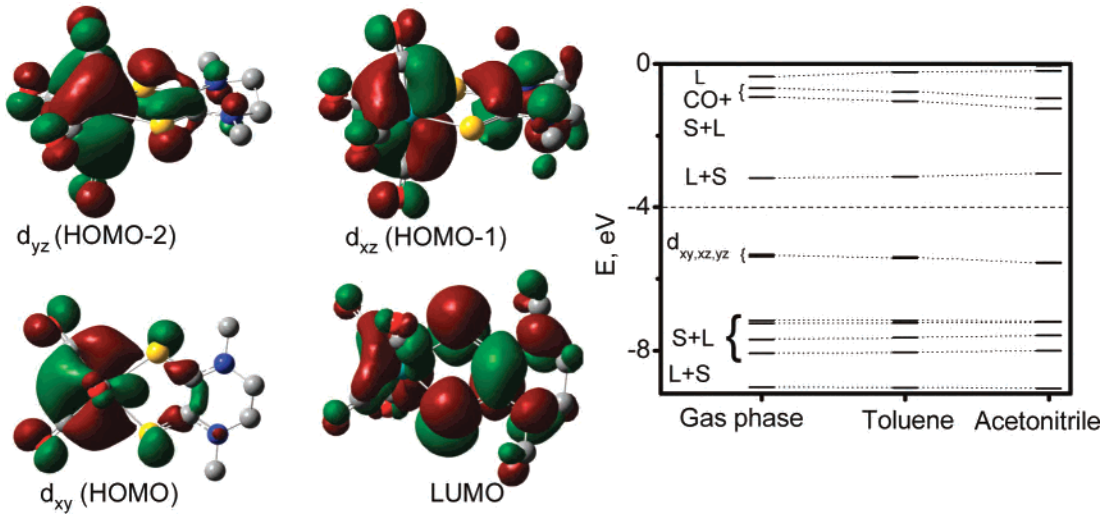

Figure 8. Selected molecular orbitals and the energy diagram of $(Me_2Pipdt)Mo(CO)_4$.

Table 5. Selected Orbital Energies and Orbital Compositions for $(Me_2Pipdt)Mo(CO)_4$ and Me_2Pipdt[a]

						$(Me_2Pipdt)Mo(CO)_4$ in the Gas Phase						
E, eV	−9.022	−8.076	−7.687	−7.248	−7.17	−5.378	−5.341	*−5.315*	−3.182	−0.926	−0.68	−0.349
Mo	0.6	17.7	11	9.2	9	63.1	56.1	*60.7*	9.6	27.5	40.5	1.9
Mo(d)	0.6	6.1	8.8	9	4.2	62.8	53.5	*59.8*	9.3	5.5	2.1	0.3
S	19.8	53.8	39.9	56.2	70.5	6.5	0.3	*9.3*	34.1	23.9	12.6	4.5
CO(ax)	0.3	0.7	8.1	2.3	0.5	12.1	13.3	*2*	6	31.3	29.9	1
CO(eq)	0.1	5	1.1	0.9	4.3	10.8	6.9	*17.4*	3.1	10.7	5.3	0.9
Me_2Pip	79.3	22.8	39.9	31.5	15.7	7.5	23.3	*10.5*	47.2	6.6	11.6	91.8
						$(Me_2Pipdt)Mo(CO)_4$ in Toluene						
E, eV	−9.042	−8.047	−7.638	−7.227	−7.171	−5.423	−5.4	*−5.384*	−3.147	−1.041	−0.78	−0.231
Mo	0.6	17.3	11.1	9.3	8.7	63	58.3	*59.8*	6.3	27.1	40.1	5.9
Mo(d)	0.5	5.8	9.1	9.1	4	62.8	56.3	*58.9*	6.2	5.9	2.4	0.4
S	20.3	53.9	41.1	56.4	71	6.4	0.8	*9.4*	33.1	23.4	12.7	7.4
CO(ax)	0.3	0.8	8.8	2.5	0.5	13.3	14.2	*1.3*	5	32.4	35.2	0.3
CO(eq)	0.1	4.8	1.2	0.9	4.1	10.8	8.3	*18.6*	2.5	10.5	5.9	1.8
Me_2Pip	78.6	23.2	37.8	30.9	15.7	6.5	18.4	*10.9*	53	6.6	6.1	84.6
						$(Me_2Pipdt)Mo(CO)_4$ in Acetonitrile						
E, eV	−9.057	−8.002	−7.579	−7.208	−7.197	−5.565	−5.547	*−5.545*	−3.055	−1.247	−0.97	−0.196
Mo	1.1	17.2	12.1	10.5	8.7	60.1	60.8	*59.5*	3.4	26.2	36.5	12.7
Mo(d)	0.7	5.7	10.2	10.5	4	59.5	60.3	*58.2*	3.2	6.2	2.9	0.7
S	21.9	53.5	42.4	56.3	71.9	8.1	8.5	*2.7*	30.6	22.8	12.3	11.1
CO(ax)	0.3	0.9	9.4	2.9	0.5	6.1	7.7	*14.7*	3.9	33.7	40.6	0.3
CO(eq)	0.4	4.6	1.5	1.1	3.9	16.3	15.5	*10*	1.8	10.6	6.4	3.4
Me_2Pip	76.3	23.9	34.6	29.1	15	9.4	7.5	*13.1*	60.3	6.7	4.2	72.5
						Me_2Pipdt in the Gas Phase						
E, eV	−10.452	−9.906	−9.782	−8.701	−6.62	−6.351	−5.878	*−5.517*	−2.08	−0.124	0.344	1.111
S	38.4	55.7	44.3	12.6	44.7	59	74.2	*74.3*	32	19.7	0.6	0.3
Me_2Pip	61.6	44.3	55.7	87.4	55.3	41	25.8	*25.7*	68	80.3	99.4	99.7

[a] HOMO orbitals are given in italics.

and metal-centered orbitals. This description is in good agreement with the earlier Xα calculations.[25,28]

For molybdenum complexes with a $(d_{xy})^n$ ground state, it is expected that the HOMO will result from the interaction of the in-plane molecular orbital of the ligand and the d_{xy} atomic orbital of the molybdenum atom. Indeed, the calculated HOMO of $(Me_2Pipdt)Mo(CO)_4$ predominantly consists of a molybdenum d_{xy} atomic orbital, which shows antibonding interaction of pseudo-σ bonds with the in-plane π orbitals of sulfur atoms as well as d−π interactions with the equatorial carbonyl ligands (Figure 8 and Table 5). The HOMO-1 and HOMO-2 predominantly consist of molybdenum d_{xz} and d_{yz} atomic orbitals with significant contributions from carbonyl π orbitals. These three nearly degenerate orbitals are energetically well-separated from the other doubly occupied orbitals. The HOMO and the two lower nearly degenerate orbitals are dominated by molybdenum atomic orbitals, which is consistent with a $4d^6$ electronic configuration of the metal ion. Taken together, the electronic structure, IR and NMR spectra, and X-ray crystallographical results suggest that molybdenum in $(Me_2Pipdt)Mo(CO)_4$ is zerovalent.

The next group important for the observed electronic spectra of $(Me_2Pipdt)Mo(CO)_4$ occupied molecular orbitals have significant sulfur atom contributions (Tables 5 and S5 in the Supporting Information). The LUMO is primarily a ligand-based antibonding π orbital localized on the S═C−C═S fragment. This orbital is about 2 eV lower in

energy than the other unoccupied molecular orbitals. The LUMO+1, +2, +4, and +6 orbitals are predominantly composed of antibonding orbitals of the axial and equatorial carbonyl ligands, while LUMO+3, +5, and +7 orbitals are practically pure antibonding orbitals of the Me_2Pipdt ligand. The molybdenum $d_{x^2-y^2}$ and d_{z2} orbitals are much higher in energy and are delocalized over several molecular orbitals with large contributions to LUMO+14 and LUMO+19 orbitals, respectively. Thus, the molybdenum-based 4d orbitals follow the order $d_{yz} < d_{xz} < d_{xy}$(HOMO) $< d_{x2-y2} < d_{z2}$. The same description essentially holds for the gas and solution phases, although occupied orbitals become slightly more stable and unoccupied orbitals become slightly less stable in solution. As a result, the HOMO−LUMO energy gap increases from the gas phase (2.133 eV) to toluene (2.237 eV) to acetonitrile (2.490 eV).

The electronic spectra of ligands similar to Me_2Pipdt and respective transition-metal complexes have been discussed on the basis of Fenske−Hall and Xα calculations using higher symmetry models.[25,28] For instance, in the *cis*-dithiooxamide ligand with C_{2v} symmetry, low-intensity $n \rightarrow \pi^*$ ($a_1 \leftarrow b_2$, HOMO-1 → LUMO) and higher-intensity $\pi \rightarrow \pi^*$ ($a_2 \leftarrow b_2$, HOMO-2 → LUMO) transitions are allowed, while the lowest-energy HOMO → LUMO ($b_1 \leftarrow b_2$) $n \rightarrow \pi^*$ transition is symmetry-forbidden, which is consistent with the experimental data.[25,26,28] Easing the symmetry restrictions, however, can increase the intensity of the last transition. For example, the electronic spectrum of Me_2pipdt consists of a broad low-intensity band at ∼500 nm and two more intense bands at 410 and 316 nm. To understand the nature of these bands, TDDFT calculations have been conducted on the geometry-optimized structure of Me_2Pipdt. Table S6 and Figure S5 in the Supporting Information compare the calculated and experimental excitation energies in the 250−700-nm region. The low-intensity band at 500 nm can be assigned predominantly to the HOMO → LUMO $n \rightarrow \pi^*$ transition, while the higher-intensity band located at 410 nm is due to the HOMO-1 → LUMO transition (second $n \rightarrow \pi^*$ excitation). The most intense band of Me_2pipdt located at 316 nm is, probably, a superposition of several transitions with close energies. The first component belongs to the first $\pi \rightarrow \pi^*$ transition (HOMO-2 → LUMO), which is similar to that observed in dithiooxamides described in the literature.[25,28] Interestingly, the presence of a second $\pi \rightarrow \pi^*$ transition (HOMO-3 → LUMO) in the valence region, for highly symmetric *cis*-dithiooxamide, has also been considered but was ruled out on the basis of the large energy difference between the HOMO-2 and HOMO-3 orbitals.[28] In our case, however, this most intense transition is relatively close in energy to the first $\pi \rightarrow \pi^*$ transition and thus may play a dominant role in the formation of the band located at 316 nm. The next two transitions ($n \rightarrow \pi^*$ in nature) are due to the HOMO → LUMO+1 and HOMO-1→ LUMO+1 excitations, which can contribute to the intensity of the band at 316 nm. Overall, the TDDFT calculations suggest that the band at 316 nm probably consists of a superposition of two $\pi \rightarrow \pi^*$ and two $n \rightarrow \pi^*$ transitions.

The optical spectra of the $(Me_2Pipdt)Mo(CO)_4$ complex in different solvents consist of an intense low-energy band in the visible region, observed between 600 and 700 nm, followed by a band at 380 nm, an intense band at ∼310 nm, and a band at ∼270 nm (when observed). Unlike the low-energy band, the other bands are only slightly solvatochromic. In addition, in the electronic spectra of $(Me_2Pipdt)Mo(CO)_4$ in THF, pyridine, DMSO, and DMF, an additional shoulder at ∼480 nm could be located. It is commonly thought that, in the case of low-valent transition-metal complexes of dithiooxamides, the intense MLCT band appears in the visible region, while the intraligand (IL) $\pi \rightarrow \pi^*$, $n \rightarrow \pi^*$, other MLCT, and ligand-field bands appear in the UV region. The calculated vertical excitation energies of $(Me_2Pipdt)Mo(CO)_4$ are presented in Tables 6 and S7 in the Supporting Information and graphically in Figures 9 and 10. Because we are interested primarily in the valence-region excitation energies,[66] we used the DZVP basis set for the molybdenum and the 6-311G(d) basis set for all other atoms.[41−43] For gas-phase calculations, the agreement between the computed and experimental excitation energies is generally good, although they are slightly overestimated for the visible region. Clearly, the low-energy band has MLCT character and consists of three transitions involving electron excitation from molybdenum d_{xy} (HOMO), d_{xz} (HOMO-1), and d_{yz} (HOMO-2) orbitals to sulfur-containing ligand-centered LUMO π^* orbital. It is interesting to note, however, that HOMO → LUMO and HOMO-2 → LUMO transitions (transitions 1 and 2) have negligible intensity, while the HOMO-1 (molybdenum d_{xz} orbital) → LUMO transition is the primary contributor to the shape of the low-energy band. One of the possible reasons for this observation is the nearly zero overlap between HOMO or HOMO-2 and LUMO orbitals, while significant overlap is expected between the HOMO-1 and LUMO orbitals. The observed shoulder at ∼380 nm can be described as a superposition of five MLCT excitations from the metal-centered occupied orbitals (d_{xy}, d_{xz}, and d_{yz}) to LUMO+1 and LUMO+2 π^* unoccupied orbitals and two IL $\pi-\pi^*$ transitions involving the LUMO orbital. The major contributors to the intense band observed at ∼310 nm are two excitations (excitations 12 and 13) that belong to IL $\pi-\pi^*$ and MLCT transitions, respectively. The band at ∼270 nm is due to a superposition of the most intense excitations (excitations 15 and 16) with MLCT character. The calculated energy gap between occupied (d_{xy}, d_{xz}, and d_{yz}) and unoccupied (d_{x2-y2} and d_{z2}) molybdenum-centered orbitals is at least 6.33 eV, which makes it difficult to observe any $d \rightarrow d$ transitions in UV−vis spectra of $(Me_2Pipdt)Mo(CO)_4$. Taken together, the TDDFT calculations indicate dominance of MLCT contributions to the electronic absorption spectrum of $(Me_2Pipdt)Mo(CO)_4$, while IL transitions contribute significantly only to bands at 310 and 270 nm.

(66) For calculating the high-energy Rydberg state transitions that involve low-energy occupied and high-energy unoccupied orbitals, accurate descriptions of diffuse molecular orbitals are often required. Sometimes this necessitates the inclusion of diffuse basis functions. Because we are interested in the valence region, which involves only valence electrons, it is not necessary to include diffuse functions in the basis set.

Table 6. Selected List of Calculated by TDDFT Excitation Energies of the $(Me_2Pipdt)Mo(CO)_4$ Complex[a]

	λ, nm (f, $\times 10^3$)	major contributions
	In the Gas Phase	
1	989.9 (0.3)	95 (d_{xy}, HOMO) → 96 (π^*, LUMO), MLCT
2	902.8 (0.3)	93 (d_{yz}) → 96 (π^*, LUMO), MLCT
3	623.9 (205.3)	94 (d_{xz}) → 96 (π^*, LUMO), MLCT
4	423.3 (0.0)	92 (n) → 96 (π^*, LUMO), IL
12	303.8 (30.8)	90 (π) → 96 (π^*, LUMO), IL
13	299.5 (32.2)	93 (d_{yz}) → 100 (π^*), 94 (d_{xz}) → 98 (π^*), MLCT
15	285.3 (13.6)	94 (d_{xz}) → 99 (π^*), MLCT
16	278.0 (137.8)	93 (d_{yz}) → 99 (π^*), MLCT
	In Toluene (Nonequilibrium)	
1	885.4 (0.3)	95 (d_{xy}, HOMO) → 96 (π^*, LUMO), MLCT
2	829.8 (0.4)	93 (d_{yz}) → 96 (π^*, LUMO), MLCT
3	645.7 (237.8)	94 (d_{xz}) → 96 (π^*, LUMO), MLCT
4	418.3 (0.1)	92 (n) → 96 (π^*, LUMO), IL
12	306.3 (80.5)	90 (π) → 96 (π^*, LUMO), IL
13	303.2 (62.0)	93 (d_{yz}) → 100 (π^*), 94 (d_{xz}) → 98 (π^*), MLCT
18	273.7 (20.8)	94 (d_{xz}) → 99 (π^*), 93 (d_{yz}) → 101 (π^*), MLCT
19	271.7 (186.8)	93 (d_{yz}) → 99 (π^*), MLCT
20	259.8 (116.7)	93 (d_{yz}) → 100 (π^*), MLCT
	In Toluene (Equilibrium)	
1	885.5 (0.3)	95 (d_{xy}, HOMO) → 96 (π^*, LUMO), MLCT
2	829.9 (0.4)	93 (d_{yz}) →96 (π^*, LUMO), MLCT
3	647.3 (242.0)	94 (d_{xz}) → 96 (π^*, LUMO), MLCT
4	418.3 (0.1)	92 (n) → 96 (π^*, LUMO), IL
12	306.5 (82.5)	90 (π) → 96 (π^*, LUMO), IL
13	303.3 (64.3)	93 (d_{yz}) → 100 (π^*), 94 (d_{xz}) → 98 (π^*), MLCT
18	273.7 (21.4)	94 (d_{xz}) → 99 (π^*), 93 (d_{yz}) → 101 (π^*), MLCT
19	271.8 (190.0)	93 (d_{yz}) → 99 (π^*), MLCT
20	260.0 (120.7)	93 (d_{yz}) → 100 (π^*), MLCT
	In Acetonitrile (Nonequilibrium)	
1	722.5 (0.2)	93 (d_{yz}) → 96 (π^*, LUMO), 94 (d_{xy}) → 96 (π^*, LUMO), MLCT
2	701.0 (0.6)	93 (d_{yz}) → 96 (π^*, LUMO), 94 (d_{xy}) → 96 (π^*, LUMO), MLCT
3	604.0 (174.8)	95 (d_{xz}, HOMO) → 96 (π^*, LUMO), MLCT
4	401.2 (0.5)	92 (n) → 96 (π^*, LUMO), IL
12	306.6 (55.4)	94 (d_{yz}) → 100 (π^*), 95 (d_{xz}), 98 (π^*), MLCT
13	303.5 (111.3)	90 (π) → 96 (π^*, LUMO), IL
18	267.2 (15.8)	95 (d_{yz}) → 99 (π^*), MLCT
19	264.0.3 (144.5)	94 (d_{xy}) → 99 (π^*), 93 (d_{yz}) → 99 (π^*), MLCT
20	262.4 (85.2)	94 (d_{xy}) → 100 (π^*), 93 (d_{yz}) → 100 (π^*), MLCT
	In Acetonitrile (Equilibrium)	
1	723.2 (0.3)	93 (d_{yz}) → 96 (π^*, LUMO), 94 (d_{xy}) → 96 (π^*, LUMO), MLCT
2	703.5 (0.9)	93 (d_{yz}) → 96 (π^*, LUMO), 94 (d_{xy}) → 96 (π^*, LUMO), MLCT
3	629.1 (262.2)	95 (d_{xz}, HOMO) → 96 (π^*, LUMO), MLCT
4	402.2 (0.7)	92 (n) → 96 (π^*, LUMO), IL
12	310.5 (137.7)	94 (d_{yz}) → 100 (π^*), 95 (d_{xz}) → 98 (π^*), MLCT
13	309.0 (179.6)	90 (π) → 96 (π^*, LUMO), IL
18	267.9 (77.7)	95 (d_{yz}) → 99 (π^*), MLCT
19	266.1 (218.7)	94 (d_{xy}) → 99 (π^*), 93 (d_{yz}) → 99 (π^*), MLCT
20	266.0 (134.4)	94 (d_{xy}) → 100 (π^*), 93 (d_{yz}) → 100 (π^*), 95 (d_{yz}) → 99 (π^*), MLCT

[a] MLCT = metal-to-ligand charge transfer. IL = intraligand.

The solvent effects in $(Me_2Pipdt)Mo(CO)_4$ were modeled using the PCM approach in conjunction with TDDFT with both equilibrium and nonequilibrium algorithms.[35,67] The nonequilibrium approach reflects a situation in which a part of the solvent polarization remains frozen similar to the initial state when a solute undergoes electronic transition. In this approach, the ratio between the dielectric constant and the square of the refractive index provides the fraction of solvent polarization capable of rearranging during the excitation, which has a large effect on the calculated excitation energies.[67] The negative solvatochromism for the ~600-nm band as well as the smaller positive solvatochromism for

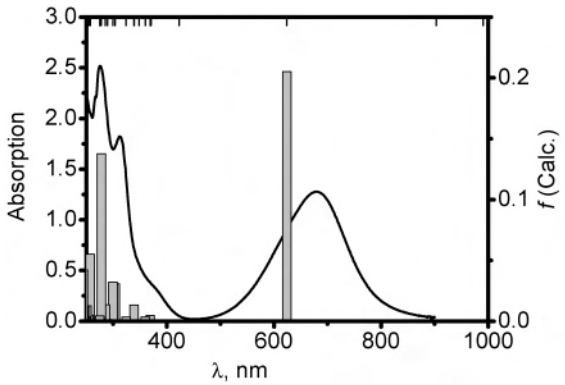

Figure 9. Experimental UV−visible spectra in DCM and calculated (gas phase) transitions for $(Me_2Pipdt)Mo(CO)_4$.

(67) Aquilante, F.; Cossi, M.; Crescenzi, O.; Scalmani, G.; Barone, V. *Mol. Phys.* **2003**, *101*, 1945−1953.

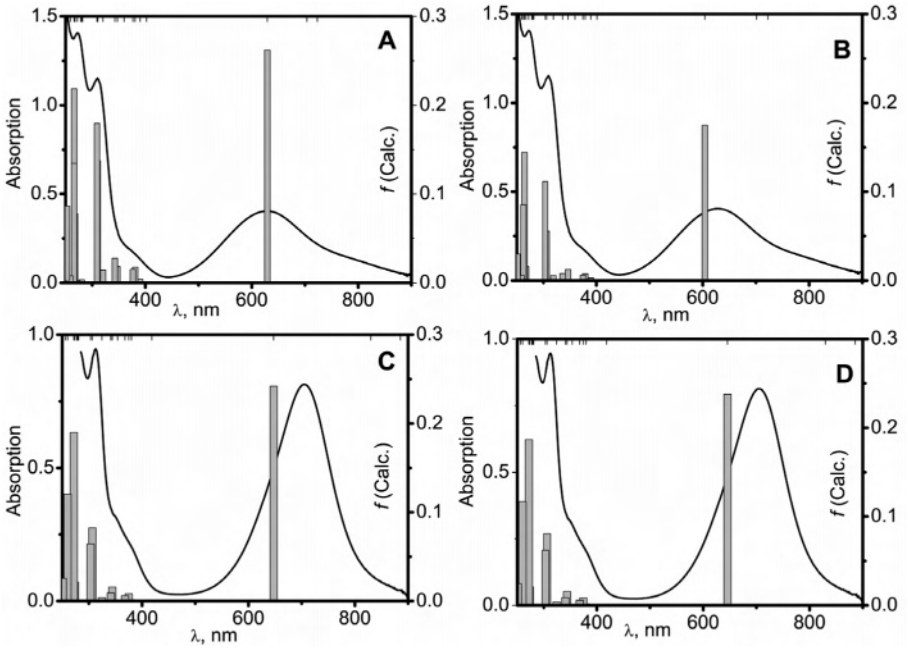

Figure 10. Experimental optical spectra and calculated (TDDFT) transition energies of the $(Me_2Pipdt)Mo(CO)_4$ complex in acetonitrile (A, equilibrium approach; B, nonequilibrium approach) and toluene (C, equilibrium approach; D, nonequilibrium approach).

the ~310-nm band are reproduced well by the TDDFT-PCM calculations, with errors consistent with other TDDFT calculations.[41,43,68] Both equilibrium and nonequilibrium models provide similar TDDFT results in toluene (Table 6), which is not surprising because toluene has a low dielectric constant. The situation is slightly different in the case of acetonitrile. In this case, the equilibrium model gives better agreement with the experimental data compared to the nonequilibrium approach for bands located at ~600 and ~310 nm (Table 6 and Figure 10), which underscores the importance of the solvent polarization effect on the calculated vertical excitation energies. It is important to note that the main contributor to the intensity of the low-energy band both in gas and solution phases is the $d_{xz} \rightarrow \pi^*$(LUMO) excitation. The d_{xz} orbital, however, is HOMO-1 in the case of the gas phase and toluene solution, while it is HOMO in the case of the acetonitrile solution. Taking into consideration that molybdenum-centered d_{xy}, d_{xz}, and d_{yz} orbitals in $(Me_2Pipdt)Mo(CO)_4$ are nearly degenerate, the small geometrical changes predicted in acetonitrile can cause intercrossing of HOMO and HOMO-1.

In general, the solvent effect can be separated into two major contributions: one reflects the geometric relaxation in a particular solvent, and the other one is the polarization induced by the solvent.[67] The effect of the first contribution can be estimated by comparing the excitation energies calculated in the gas phase using the gas- and solution-phase geometries. The second effect can be estimated by calculating the excitation energies in the gas phase and in solution with a fixed geometry optimized in the solution. Finally, the polarization effect between different solvents can be estimated as a difference between the calculated excitation energies in toluene and in acetonitrile using geometry optimized in acetonitrile. Our results for the geometry relaxation effect contribute a maximum of −0.1014 eV for the first MLCT band (first three transitions). On the other hand, the calculated maximum polarization effect for the acetonitrile solution is +0.4898 eV for the first transition, while it is +0.1665 eV for the most intense low-energy $d_{xz} \rightarrow$ LUMO excitation. The total shift calculated for acetonitrile is +0.0651 eV for the most intense low-energy $d_{xz} \rightarrow$ LUMO excitation and +0.3884 eV as the maximum shift. The estimated polarization effect between toluene and acetonitrile solutions has been calculated to be +0.1545 eV for the $d_{xz} \rightarrow$ LUMO excitation.

(68) Wang, F.; Ziegler, T. *Mol. Phys.* **2004**, *102*, 2585−2595.

Conclusions

In this paper, we report the synthesis and spectroscopic and structural characterization of $(Me_2Pipdt)Mo(CO)_4$ (Me_2Pipdt = *N*,*N*′-piperazine-2,3-dithione). The two independent molecules in the unit cell show a small change in the NC(S)C(S)N dihedral angles (11.2 and 12.9°), which is significantly different from that of the free ligand (35°). The spectroscopic data (^1H and ^{13}C NMR and IR) and DFT calculations clearly suggest the presence of the oxidized dithione form of the sulfur-containing ligand. In general, calculated gas- and solution-phase geometries compare well with the experimental values, although the flexible NC(S)C(S)N fragment exhibits a large variation in the torsion angle. The HOMO to HOMO-2 orbitals of $(Me_2Pipdt)Mo(CO)_4$ are nearly degenerate and predominantly consist of molybdenum 4d orbitals with near-equal contributions from the dithione and carbonyl ligands. The LUMO orbital is energetically well-isolated and is practically a pure π^* orbital localized on the C═S fragment. TDDFT-PCM calculations correctly predict negative solvatochromism and magnitude of the solvent shift for the lowest-energy MLCT band in the

electronic spectra of $(Me_2Pipdt)Mo(CO)_4$. The major contribution to this band is the $d_{xz} \rightarrow$ LUMO transition, while the d_{xy} and $d_{yz} \rightarrow$ LUMO transitions have negligibly small intensities. In general, MLCT bands are dominated over dithiooxamide ligand $\pi-\pi^*$ transitions not only in the visible but also in the UV region.

Acknowledgment. Generous computing time offered by the University of Minnesota Supercomputing Institute to V.N.N. is appreciated. Partial financial support of this research by the National Institutes of Health (Grant GM 615502) to P.B. is gratefully acknowledged.

Supporting Information Available: Crystallographic data in CIF format and tables and figures of atomic coordinates, IR frequencies, DFT and TDDFT calculated energies, and full molecular orbital compositions. This material is available free of charge via the Internet at http://pubs.acs.org.

IC051653P